AC transport in correlated quantum dots: From Kondo to Coulomb blockade regime

G. Stefanucci[1,2] and S. Kurth[3,4,5]

[1]*Dipartimento di Fisica and European Theoretical Spectroscopy Facility (ETSF), Università di Roma Tor Vergata, Via della Ricerca Scientifica 1, 00133 Rome, Italy*

[2]*INFN, Laboratori Nazionali di Frascati, Via E. Fermi 40, 00044 Frascati, Italy*

[3]*Nano-Bio Spectroscopy Group and European Theoretical Spectroscopy Facility (ETSF), Departamento de Física de Materiales, Universidad del País Vasco UPV/EHU, Avenida Tolosa 72, E-20018 San Sebastián, Spain*

[4]*IKERBASQUE, Basque Foundation for Science, Maria Diaz de Haro 3, E-48013 Bilbao, Spain*

[5]*Donostia International Physics Center (DIPC), Paseo Manuel de Lardizabal 4, E-20018 San Sebastián, Spain*

(Received 19 October 2017; published 18 June 2018)

We explore the finite-bias DC differential conductance of a correlated quantum dot under the influence of an AC field, from the low-temperature Kondo to the finite-temperature Coulomb blockade regime. Real-time simulations are performed using a time-dependent generalization of the steady-state density functional theory (i-DFT) [Nano Lett. **15**, 8020 (2015)]. The numerical simplicity of i-DFT allows for unprecedented long time evolutions. Accurate values of average current and density are obtained by integrating over several periods of the AC field. We find that (i) the zero-temperature Kondo plateau is suppressed, (ii) the photon-assisted conductance peaks are shifted due to correlations, and (iii) the Coulomb blockade is lifted with a concomitant smoothening of the sharp diamond edges.

DOI: 10.1103/PhysRevB.97.245415

I. INTRODUCTION

In recent decades there have been tremendous advances in manufacturing nanoscale devices such as nanotubes, artificial atoms (quantum dots), and single molecules attached to metallic leads [1–4]. The theoretical description of their transport properties often remains a challenge since it involves the physics of strong correlations out of thermal equilibrium. Even the (minimal) single impurity Anderson model [5] (SIAM) after almost sixty years is still a matter of intense research and debate. A fairly good understanding of its equilibrium and steady state properties has evolved through the development of clever analytical and numerical techniques which agree reasonably well among each other [6]. On the other hand, devising techniques and algorithms to study time-dependent responses is still an active field of research (see discussion below). In particular, relatively little is known about the behavior of the average current when an AC bias is superimposed on a DC voltage [7,8]. What is the fate of the zero-temperature Kondo plateau in the conductance? How does the charging energy affect the photon-assisted conductance peaks? Is the finite-temperature Coulomb blockade lifted? In this paper we provide an answer to these and related fundamental questions.

One way to access AC (linear as well as nonlinear) transport properties consists in performing numerical simulations of the time-evolution of the system. Several time-propagation algorithms have been put forward. Time-dependent (TD) density matrix renormalization group [9–13], TD numerical renormalization group [14], functional renormalization group [6,15,16], real-time Monte Carlo [17–21], hierarchical equations of motion [22], iterative real-time path integral [23], and real-time effective action [24] approaches have all been used to investigate the transient response to a sudden quench of bias or gate voltages, and a reasonable agreement between them has been reached. These methods, however, are limited to short propagation times, and AC responses are difficult to address since convergence often requires averaging the TD current over several periods of the driving field. An alternative to time propagation is the Floquet Green's function approach, which has been used to study responses to an oscillating *gate* in Refs. [25–27].

Lately, strongly correlated systems have been studied also with density functional theory (DFT) in both its static [28–32] and time-dependent [33–38] versions. In a recent work we proposed a steady-state density functional theory [39] (i-DFT) to calculate the steady density on and the steady current through a quantum junction sandwiched between metallic leads. In Ref. [40] we applied i-DFT to the SIAM and found excellent agreement with numerically accurate methods in a wide range of bias and gate voltages, from weak to strong charging energies U and from low to high temperatures T.

We here extend i-DFT to the time domain, thereby laying down a computationally feasible scheme to shed light on the AC transport properties of the SIAM. Our main findings are (i) AC voltage suppression of the $T = 0$ Kondo plateau, (ii) interaction-induced shift of the photon-assisted conductance peaks, and (iii) lifting of the finite-temperature Coulomb blockade with concomitant smoothening of the diamond shape.

II. TIME-DEPENDENT i-DFT

i-DFT establishes a one-to-one correspondence between the pair density on and current through the impurity, (n, I), and the pair gate and bias voltages (v, V). Accordingly, there exists a unique pair (v_s, V_s) that in the noninteracting SIAM produces the same density and current as in the interacting one. We stress

that except for n and I all other physical quantities, e.g., the transverse current, the lead density, or the spectral function, are in general different in the noninteracting and interacting SIAM. The pair (v_s, V_s) consists of the Kohn-Sham (KS) gate $v_s = v + v_{\rm H} + v_{\rm xc}$ and KS voltage $V_s = V + V_{\rm xc}$, where the Hartree (H) potential $v_{\rm H} = Un$ whereas the exchange-correlation (xc) potentials $v_{\rm xc}$ and $V_{\rm xc}$ are universal functionals (i.e., independent of the external fields v and V) of both density and current. Knowledge of these functionals allows for calculating (n, I) by solving self-consistently the equations

$$n = 2\sum_{\alpha=L,R}\int \frac{d\omega}{2\pi} f(\omega - V_{s,\alpha}) A_\alpha(\omega), \tag{1}$$

$$I = 2\int \frac{d\omega}{2\pi}[f(\omega - V_{s,L}) - f(\omega - V_{s,R})]\mathcal{T}(\omega), \tag{2}$$

where $V_{s,L} = -V_{s,R} = V_s/2$ is the bias applied to the left (L) and right (R) leads and $f(\omega) = 1/(e^{\beta(\omega-\mu)} + 1)$ is the Fermi function at inverse temperature $\beta = 1/T$ and chemical potential μ. In Eq. (1) the partial spectral function is given by $A_\alpha(\omega) \equiv G(\omega)\Gamma_\alpha(\omega)G^\dagger(\omega)$ with the (retarded) KS Green's function $G(\omega) = 1/[\omega - v - v_{\rm Hxc} - \Sigma_L(\omega) - \Sigma_R(\omega)]$ and broadening $\Gamma_\alpha(\omega) = -2\,{\rm Im}[\Sigma_\alpha(\omega)]$, Σ_α being the embedding self-energy of lead α. The current in Eq. (2) is expressed in terms of the KS transmission coefficient $\mathcal{T}(\omega) = A_L(\omega)\Gamma_R(\omega)$. The self-consistent solution of Eqs. (1) and (2) is extremely efficient [40,41]. It is therefore natural to extend i-DFT to the time domain and explore dynamical (as opposed to steady-state) transport properties. Setting the external bias $V(t) = \theta(t)[V + V_{\rm AC}\sin(\Omega t)]$ we can provide a full characterization of the AC conductance.

In the same spirit of the adiabatic approximations in standard TD-DFT [42,43] we calculate the TD density $n(t)$ and current $I(t)$ by propagating the KS SIAM with TD gate potential $v_s(t) = v(t) + v_{\rm Hxc}[n(t), I(t)]$ and voltage $V_s(t) = V(t) + V_{\rm xc}[n(t), I(t)]$. The adiabatic approximation is, by construction, accurate for slowly varying external fields, whereas it is expected to fail for ultrafast protocols like the sudden quench of a gate or bias voltage. Adiabatic TD i-DFT is therefore complementary to the aforementioned many-body methods [6,9–24] which, due to their non-negligible computational cost, are limited to short propagation times and therefore suited to investigate transient responses to ultrafast fields.

The propagation is performed by solving the coupled TD KS equation

$$i\frac{d}{dt}\begin{pmatrix}\psi_{L,k}\\ \psi_{C,k}\\ \psi_{R,k}\end{pmatrix} = \begin{pmatrix}h_{LL} & h_{LC} & 0\\ h_{CL} & h_{CC} & h_{CR}\\ 0 & h_{RC} & h_{RR}\end{pmatrix}\begin{pmatrix}\psi_{L,k}\\ \psi_{C,k}\\ \psi_{R,k}\end{pmatrix} \tag{3}$$

for every KS state ψ_k. Equation (3) is written in a block form where the blocks L and R refer to the left and right leads whereas the block C refers to the impurity site, hence $h_{CC} = v_s(t)$. We model the leads as semi-infinite tight-binding chains with nearest-neighbor hopping $t_{\rm lead}$ and onsite energy $V_{s,\alpha}(t)$. Only the boundary site of the semi-infinite chains is connected to the impurity, and the corresponding hopping amplitude is $t_{\rm link}$. We take the leads at half-filling ($\mu = 0$), choose both $t_{\rm lead}$ and $t_{\rm link}$ much larger than any other energy scale and set the ratio $t_{\rm link}^2/t_{\rm lead} = \gamma/2$ to stay in the wide band limit (WBL).

Equation (3) is solved using a generalization of the algorithm of Ref. [44] to finite temperatures. The time propagation is performed with a predictor-corrector scheme at each time step for $v_{\rm Hxc}$ and $V_{\rm xc}$. The TD occupation and current to plug into the xc potentials are obtained from the KS wave functions according to

$$n(t) = 2\sum_k f(\epsilon_k)|\psi_{C,k}(t)|^2, \tag{4}$$

$$I(t) = \frac{I_L(t) - I_R(t)}{2}. \tag{5}$$

The current at the α interface,

$$I_\alpha(t) = 4\sum_k f(\epsilon_k)\,{\rm Im}[t_{\rm link}\psi^*_{\alpha,k}(t)\psi_{C,k}(t)], \tag{6}$$

is expressed in terms of the wave function $\psi_{\alpha,k}(t)$ at boundary site of lead α. Notice that current conservation implies $I_L(t) + I_R(t) + \dot n(t) = 0$ at all times. For symmetric voltages $V_L(t) = -V_R(t) = V(t)/2$ and at the particle-hole symmetric point (ph-SP) $v = -U/2$ we have $I_L(t) = -I_R(t)$.

In Ref. [40] we proposed an accurate parametrization of $v_{\rm Hxc}$ and $V_{\rm xc}$ for the SIAM symmetrically coupled to left and right leads. This parametrization has been shown to agree well with results from the functional and numerical renormalization group in a wide range of temperatures and interaction strengths. We have used the xc potentials of Ref. [40] to solve Eq. (3). A somewhat related current-dependent approximation for $v_{\rm Hxc}$, valid for only one lead and at temperatures higher than the Kondo temperature $T_{\rm K} = \frac{4}{\pi}\sqrt{U\gamma}\exp[-\frac{\pi}{4}(\frac{U}{\gamma} - \frac{\gamma}{U}v)]$, has recently been suggested in Ref. [45].

III. RESULTS

We consider the symmetrically coupled SIAM initially (times $t \leqslant 0$) in thermal equilibrium and then driven out of equilibrium by a symmetric bias $V_L(t) = -V_R(t) = V(t)/2$. The bias is the sum of a DC and an AC contribution, i.e.,

$$V(t) = V + V_{\rm AC}\sin(\Omega t) \quad \text{for } t > 0. \tag{7}$$

After a sufficiently long propagation time t_ℓ the transient features die out and all physical observables become periodic functions of time. We then calculate the DC component of the current by averaging $I(t)$ over N periods $\tau = 2\pi/\Omega$, i.e., $I_{\rm DC} = \int_{t_\ell}^{t_\ell + N\tau} {\rm d}t\, I(t)/(N\tau)$. Depending on the parameters, a good convergence may require N of the order of 10 or larger. Finally we calculate the finite-bias DC conductance $G = {\rm d}I_{\rm DC}/{\rm d}V$, highlighting its most relevant features as $V_{\rm AC}$ and Ω are varied. We consider two physically distinct regimes: the Kondo regime at zero temperature and the Coulomb blockade (CB) regime at temperatures larger than the Kondo temperature.

First we checked that for $U = V = 0$ our TD algorithm agrees with the exact (in the WBL approximation) noninteracting formula [46]

$$G^{U=0} = \sum_{k=-\infty}^{\infty} J_k^2\left(-\frac{V_{\rm AC}}{\Omega}\right)\frac{\frac{\gamma^2}{4}}{(v - k\Omega)^2 + \frac{\gamma^2}{4}}, \tag{8}$$

where $J_k(x)$ is the Bessel function of order k. Without interactions, photon-assisted transport (PAT), i.e., charge transfer

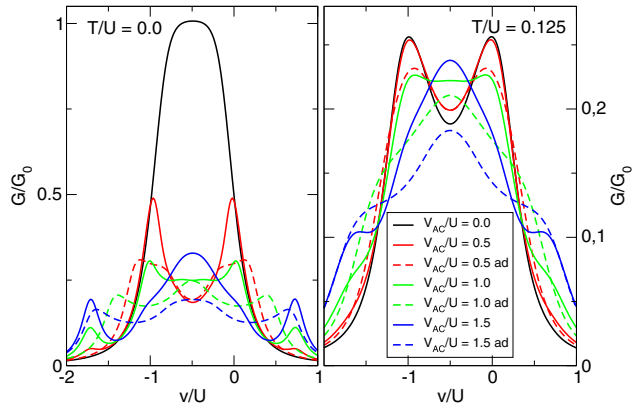

FIG. 1. Zero-bias DC conductance (solid lines) as well as its adiabatic counterpart of Eq. (9) (dashed) versus v for different AC amplitudes. The SIAM parameters are $U/\gamma = 4$ ($T_K/U = 0.033$), $\Omega/U = \pi/4$ and temperature $T = 0$ (left panel), and $T/U = 0.125$ (right panel). $G_0 = \frac{1}{\pi}$ is the quantum of conductance.

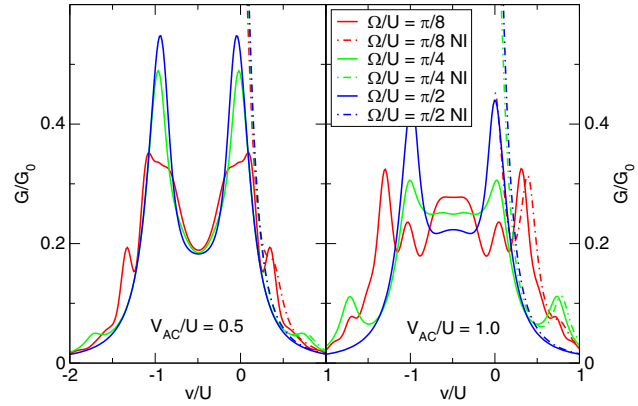

FIG. 2. Zero-bias DC conductance versus v for different AC frequencies and for amplitudes $V_{AC}/U = 0.5$ (left panel) and $V_{AC}/U = 1.0$ (right panel). Other parameters as in Fig. 1. Dashed lines: noninteracting result of Eq. (8).

accompanied by the emission or absorption of photons, is the only scattering mechanism.

Turning on the interaction, the scenario changes dramatically, especially for gates v in the range $(-U,0)$ where correlation effects are enhanced. In Fig. 1 we show results for the zero-bias DC conductance as function of v for different V_{AC}. At temperature $T = 0$ (left panel) and for $V_{AC} < U$ (but larger than T_K) the Kondo plateau is drastically suppressed. The DC conductance resembles the one at $V_{AC} = 0$ in the CB regime, with two peaks separated by roughly the charging energy U and a minimum at the ph-SP. The suppression of Kondo correlations has already been observed in Refs. [47,48] using a perturbative approach as well as in Refs. [25,27] where, rather than an AC bias, the *gate* potential is perturbed harmonically. As V_{AC} increases, however, the minimum is first converted into a plateau and eventually into a maximum with the concomitant washing out of the side peaks. The decrease and subsequent increase of the Kondo peak at the ph-SP predicted by our calculations is in agreement with experimental findings reported in Ref. [49].

In the CB regime ($T/U = 0.125$, right panel) a small AC bias barely changes the values of G at $V_{AC} = 0$. However, for $V_{AC} \approx U$ the DC conductance develops a plateau and a maximum at the ph-SP for even larger amplitudes. In both regimes, see left and right panels, we also observe increasingly higher side peaks at $v \approx \Omega$ and $v \approx -U - \Omega$ with increasing V_{AC}, a clear signature of PAT. We will discuss the precise position of these peaks below.

To highlight nonadiabatic (memory) effects we define the "adiabatic" DC conductance according to

$$G_{ad} = \frac{1}{\tau}\int_0^\tau dt\; G_{DC}(V(t)), \tag{9}$$

where $G_{DC}(V) = dI/dV|_{V_{AC}=0}$ is the finite-bias DC conductance at vanishing AC amplitude. The results for G_{ad} are shown in both panels of Fig. 1 (dashed lines). For small V_{AC} and around the ph-SP, G_{ad} is remarkably close to G both in the Kondo and the CB regime while away from ph-SP the two quantities only share qualitative features at best. For larger V_{AC}, adiabatic and nonadiabatic DC conductances increasingly differ, pointing to the importance of memory.

In Fig. 2 we show the dependence of the zero-bias G at $T = 0$ on the AC frequency for two different AC amplitudes. At the small amplitude $V_{AC}/U = 0.5$ (left panel) the behavior of G is qualitatively similar for different frequencies (suppression of the Kondo plateau and arising of PAT peaks). Interestingly, for the larger amplitude $V_{AC}/U = 1.0$ (right panel), G develops a plateau around the ph-SP *for all* frequencies, with a height that decreases monotonically with Ω. For this larger amplitude the PAT peaks emerge more distinctly and we clearly appreciate the nonlinear (in V_{AC}) effect of absorption/emission of two photons (for $\Omega/U = \pi/8$).

The dashed curves starting at $v = 0$ in both panels of Fig. 2 are the values of $G^{U=0}$, see Eq. (8) (which is an even functions of v), exhibiting PAT peaks at $v = k\Omega$ with k integer [46]. For $v > 0$, the interacting and noninteracing results agree reasonably well while for $v < 0$ correlations shift the PAT peaks by approximately $-U$.

It is worth noting that in the interacting case the PAT peak at $v \approx \Omega$ is slightly shifted to lower gates. To shed some light on this shift we calculated the zero-bias G for various charging energies U. The results are shown in the upper panel of Fig. 3, where the inset is a magnification of the PAT peak at $v \approx \Omega$. For these gate values correlations are weak as confirmed by the small value $n \approx 0.15$ of the time-averaged density; see the inset in the lower panel. In the weakly correlated regime the DC conductance is well approximated by the noninteracting formula of Eq. (8). However, from the i-DFT perspective, the v in Eq. (8) is not just the bare gate but instead the time-averaged KS gate $v_s = v + v_{Hxc}$, i.e., the sum of the bare gate and the time-averaged Hxc potential v_{Hxc} shown in the lower panel of Fig. 3. Consequently, the PAT peak in G occurs at $v = \Omega - v_{Hxc}$, i.e., it is shifted to lower energies. This is precisely the shift we observe in our calculations. In fact, if we evaluate Eq. (8) making the replacement $v \to v_s$ we get a remarkable good agreement with the *interacting* G (including position and height of the PAT peaks) for v outside the interval $(-U,0)$; see the dashed curves in the upper panel of Fig. 3. Obviously, this good agreement breaks down for gates in the

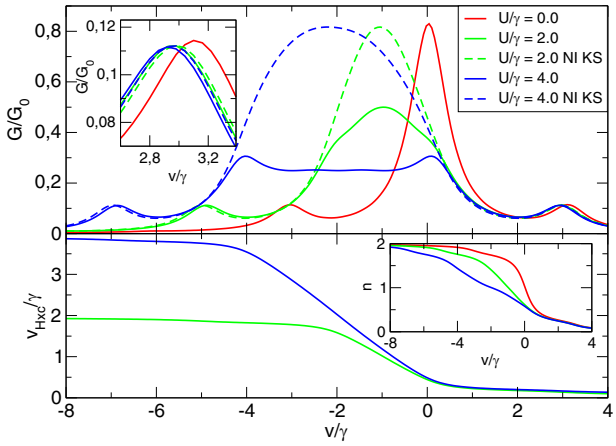

FIG. 3. Upper panel: Zero-bias DC conductances (solid) versus v for $\Omega/\gamma = \pi$, $V_{\rm AC}/\gamma = 4.0$ and for $U/\gamma = 0$, $U/\gamma = 2$ ($T_{\rm K}/U = 0.277$), and $U/\gamma = 4$ ($T_{\rm K}/U = 0.033$). Dashed lines are the non-interacting result of Eq. (8) with v replaced by the time-averaged KS potential v_s. Inset: Zoom-in around $v = \Omega$ showing shifts in the position of the PAT peak. Lower panel: Time-averaged Hxc gate and density (inset).

interval $(-U,0)$ since the system can no longer be considered weakly correlated.

So far we have presented results for the zero-bias DC conductance. However, the proposed method is not limited to this very special case. In Fig. 4 we display the finite-bias G as function of v and V for different amplitudes of the AC field. The calculations are done at temperature $T = 0$. To appreciate the effects of the AC field, the well-known pure DC result, i.e., $V_{\rm AC} = 0$, is shown in panel (a). We correctly reproduce the CB diamond as well as the Kondo resonance at $V = 0$. A moderate amplitude of the AC field, panel (b), leads to a suppression of the Kondo resonance (see also Fig. 1). Moreover, starting from the finite bias corners at $v/U = -1/2$ and $V/U = \pm 1$, the CB is lifted inside the diamond. As $V_{\rm AC}$ increases further, panels (c) and (d), the CB is lifted everywhere in the diamond, leaving for the largest amplitude, panel (d), an area of increased conductance around the ph-SP at $V = 0$. We also find that the side peaks due to PAT seen in Figs. 1 and 2 branch at finite bias into straight lines with negative and positive slopes,

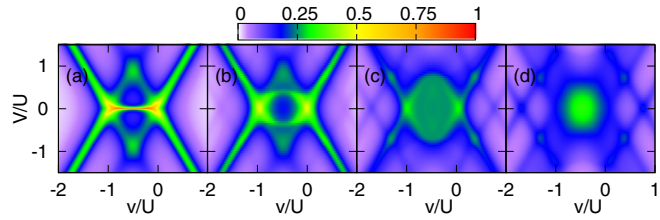

FIG. 4. DC conductance in the (v,V) plane at zero temperature for (a) $V_{\rm AC}/U = 0.0$, (b) $V_{\rm AC}/U = 0.5$, (c) $V_{\rm AC}/U = 1.0$, and (d) $V_{\rm AC}/U = 1.5$. Other parameters are as in Fig. 1.

reminiscent of the typical G lines at $V_{\rm AC} = 0$. Not surprisingly, these lines become more pronounced as $V_{\rm AC}$ increases.

IV. CONCLUSIONS

We have investigated electron transport through a correlated quantum dot subjected simultaneously to DC and AC biases by explicit and numerically efficient time propagation in a DFT framework. For the corresponding Hxc gate and xc bias potentials we have suggested a time-local approximation based on recently proposed accurate i-DFT functionals for the steady state. We find that in the Kondo regime already for small AC amplitude the Kondo plateau in the zero-bias DC conductance is strongly suppressed, while in the CB regime the changes are less pronounced. The observed shift of the photon-assisted transport peaks due to electronic interactions can readily be explained within DFT. At finite DC bias, the Coulomb blockade is lifted with increasing AC amplitude and the CB diamond is deformed.

ACKNOWLEDGMENTS

G.S. acknowledges funding by MIUR FIRB Grant No. RBFR12SW0J, EC funding through the RISE Co-ExAN (GA644076), and funding through the INFN-Nemesys project. S.K. acknowledges funding by a grant of the "Ministerio de Economia y Competividad (MINECO)" (FIS2016-79464-P) through the "Agencia Estatal de Investigación" (AEI) and the EU "Fondo Europeo de Desarrollo Regional" (FEDER) and by the "Grupos Consolidados UPV/EHU del Gobierno Vasco" (IT578-13).

[1] G. Cuniberti, G. Fagas, and K. Richter, *Introducing Molecular Electronics* (Springer, Heidelberg, 2005).
[2] Y. V. Nazarov and Y. M. Blanter, *Quantum Transport: Introduction to Nanoscience* (Cambridge University Press, Cambridge, 2009).
[3] J. C. Cuevas and E. Scheer, *Molecular Electronics: An Introduction to Theory and Experiment* (World Scientific, London, 2010).
[4] I. Baldea, *Molecular Electronics: An Experimental and Theoretical Approach* (Pan Stanford, Singapore, 2015).
[5] P. W. Anderson, Phys. Rev. **124**, 41 (1961).
[6] J. Eckel, F. Heidrich-Meisner, S. G. Jakobs, M. Thorwart, M. Pletyukhov, and R. Egger, New J. Phys. **12**, 043042 (2010).
[7] T.-K. Ng, Phys. Rev. Lett. **76**, 487 (1996).
[8] Y. Yu, T. C. Au Yeung, W. Z. Shangguan, and C. H. Kam, Phys. Rev. B **63**, 205314 (2001).
[9] K. A. Al-Hassanieh, A. E. Feiguin, J. A. Riera, C. A. Büsser, and E. Dagotto, Phys. Rev. B **73**, 195304 (2006).
[10] L. G. G. V. Dias da Silva, F. Heidrich-Meisner, A. E. Feiguin, C. A. Büsser, G. B. Martins, E. V. Anda, and E. Dagotto, Phys. Rev. B **78**, 195317 (2008).
[11] F. Heidrich-Meisner, A. E. Feiguin, and E. Dagotto, Phys. Rev. B **79**, 235336 (2009).
[12] M. Nuss, M. Ganahl, H. G. Evertz, E. Arrigoni, and W. von der Linden, Phys. Rev. B **88**, 045132 (2013).

[13] S. Kirino, T. Fujii, J. Zhao, and K. Ueda, J. Phys. Soc. Jpn. **77**, 084704 (2008).
[14] F. B. Anders and A. Schiller, Phys. Rev. Lett. **95**, 196801 (2005).
[15] S. G. Jakobs, M. Pletyukhov, and H. Schoeller, Phys. Rev. B **81**, 195109 (2010).
[16] C. Karrasch, V. Meden, and K. Schönhammer, Phys. Rev. B **82**, 125114 (2010).
[17] L. Mühlbacher and E. Rabani, Phys. Rev. Lett. **100**, 176403 (2008).
[18] A. E. Antipov, Q. Dong, and E. Gull, Phys. Rev. Lett. **116**, 036801 (2016).
[19] P. Werner, T. Oka, M. Eckstein, and A. J. Millis, Phys. Rev. B **81**, 035108 (2010).
[20] P. Werner, T. Oka, and A. J. Millis, Phys. Rev. B **79**, 035320 (2009).
[21] A. Droghetti and I. Rungger, Phys. Rev. B **95**, 085131 (2017).
[22] Y. Cheng, W. Hou, Y. Wang, Z. Li, J. Wei, and Y. Yan, New J. Phys. **17**, 033009 (2015).
[23] S. Weiss, J. Eckel, M. Thorwart, and R. Egger, Phys. Rev. B **77**, 195316 (2008).
[24] S. Bock, A. Liluashvili, and T. Gasenzer, Phys. Rev. B **94**, 045108 (2016).
[25] R. López, R. Aguado, G. Platero, and C. Tejedor, Phys. Rev. Lett. **81**, 4688 (1998).
[26] P. Nordlander, N. S. Wingreen, Y. Meir, and D. C. Langreth, Phys. Rev. B **61**, 2146 (2000).
[27] R. López, R. Aguado, G. Platero, and C. Tejedor, Phys. Rev. B **64**, 075319 (2001).
[28] K. Schönhammer, O. Gunnarsson, and R. M. Noack, Phys. Rev. B **52**, 2504 (1995).
[29] N. A. Lima, M. F. Silva, L. N. Oliveira, and K. Capelle, Phys. Rev. Lett. **90**, 146402 (2003).
[30] F. Malet and P. Gori-Giorgi, Phys. Rev. Lett. **109**, 246402 (2012).
[31] J. Lorenzana, Z.-J. Ying, and V. Brosco, Phys. Rev. B **86**, 075131 (2012).
[32] A. Mirtschink, M. Seidl, and P. Gori-Giorgi, Phys. Rev. Lett. **111**, 126402 (2013).
[33] C. Verdozzi, Phys. Rev. Lett. **101**, 166401 (2008).
[34] S. Kurth, G. Stefanucci, E. Khosravi, C. Verdozzi, and E. K. U. Gross, Phys. Rev. Lett. **104**, 236801 (2010).
[35] A.-M. Uimonen, E. Khosravi, A. Stan, G. Stefanucci, S. Kurth, R. van Leeuwen, and E. K. U. Gross, Phys. Rev. B **84**, 115103 (2011).
[36] A. Kartsev, D. Karlsson, A. Privitera, and C. Verdozzi, Sci. Rep. **3**, 2570 (2013).
[37] M. J. P. Hodgson, J. D. Ramsden, J. B. J. Chapman, P. Lillystone, and R. W. Godby, Phys. Rev. B **88**, 241102 (2013).
[38] M. J. P. Hodgson, J. D. Ramsden, and R. W. Godby, Phys. Rev. B **93**, 155146 (2016).
[39] G. Stefanucci and S. Kurth, Nano Lett. **15**, 8020 (2015).
[40] S. Kurth and G. Stefanucci, Phys. Rev. B **94**, 241103(R) (2016).
[41] S. Kurth and G. Stefanucci, J. Phys.: Condens. Matter **29**, 413002 (2017).
[42] C. Ullrich, *Time-Dependent Density-Functional Theory* (Oxford University Press, Oxford, 2012).
[43] N. T. Maitra, J. Chem. Phys. **144**, 220901 (2016).
[44] S. Kurth, G. Stefanucci, C.-O. Almbladh, A. Rubio, and E. K. U. Gross, Phys. Rev. B **72**, 035308 (2005).
[45] N. Dittmann, J. Splettstoesser, and N. Helbig, Phys. Rev. Lett. **120**, 157701 (2018).
[46] A.-P. Jauho, N. S. Wingreen, and Y. Meir, Phys. Rev. B **50**, 5528 (1994).
[47] Y. Goldin and Y. Avishai, Phys. Rev. Lett. **81**, 5394 (1998).
[48] Y. Goldin and Y. Avishai, Phys. Rev. B **61**, 16750 (2000).
[49] J. M. Elzerman, S. De Franceschi, D. Goldhaber-Gordon, W. G. van der Wiel, and L. P. Kouwenhoven, J. Low Temp. Phys. **118**, 375 (2000).